

Incompressible Flow over Airfoils

Of the many problems now engaging attention, the following are considered of immediate importance and will be considered by the committee as rapidly as funds can be secured for the purpose.... The evolution of more efficient wing sections of practical form, embodying suitable dimensions for an economical structure, with moderate travel of the center-of-pressure and still affording a large range of angle-of-attack combined with efficient action.

**From the first Annual Report of the
NACA, 1915**

PREVIEW BOX

Imagine that you have just been given an airfoil of a particular shape at a certain angle of attack to a given low-speed flow, and you have been asked to obtain the lift (or more importantly, the lift coefficient) of the airfoil. What do you do (besides panicking)? Your first inclination might be to make a model of the airfoil, put it in a low-speed wind tunnel, and measure the lift coefficient. This is indeed what aerodynamicists have been doing for more than 100 years. The early part of this chapter discusses such experimental measurements of airfoil properties in low-speed wind tunnels. These measurements give you an immediate feel for airfoil lift, drag, and moment coefficients as

a function of angle of attack. The experimental measurements give you a fast track towards obtaining a comfortable and practical understanding as to how airfoils behave. That is what the first three sections of this chapter are all about.

Most of the rest of this chapter, however, deals with our second inclination as to how to obtain the airfoil properties, namely, to *calculate* them. This is a horse of a different color. You will be introduced to the elegant circulation theory of lift—the crowning jewel of inviscid, incompressible flow theory for the calculation of lift. At the turn of the twentieth century, the circulation theory of lift was a breakthrough

in the theoretical prediction of lift. In this chapter, we first apply this theory to thin airfoils at small angles of attack; thin airfoil theory was developed in Germany during World War I and is by far the most tractable means of obtaining analytical solutions for lift and moments on an airfoil. But, as we shall see, thin airfoil theory, as its name implies, holds only for thin airfoils at small angles of attack. This is not as restrictive as it seems, however, because many airplanes over the past years have relatively thin airfoils, and cruise at relatively small angles of attack. Thin airfoil theory gives us a lot of practical results, plus the intellectual gratification of carrying through some elegant theoretical thinking—give it a good read and I think you will like it.

Since the 1960s, the advent and development of the high-speed digital computer allowed detailed numerical solutions based on the circulation theory of lift, solutions for the lift on a body of arbitrary shape and thickness at any angle of attack, subject of course to the assumption of inviscid potential flow. These numerical solutions, an extension of the panel solutions discussed in Section 3.17, are discussed towards the end of this chapter—they are the “gold standard” for low-speed, inviscid-flow airfoil calculations, and are used throughout the aeronautical industry and by many aeronautical research and development laboratories. The concept of panel solutions is an inspired numerical application of the circulation theory of lift, and it has opened the door to the analysis of practically any airfoil shape at any angle of attack.

Airfoils come in many different shapes. An historical sequence of airfoil shapes through 1935 is shown in Figure 4.1. Beginning in 1938, the National Advisory Committee for Aeronautics (NACA) developed a revolutionary series of airfoil shapes designed to encourage laminar flow in the boundary layer over the airfoil, hence dramatically reducing skin friction drag on the airfoil; the shape of a representative laminar-flow airfoil is given in Figure 4.2. Although these shapes never produced the desired amount of laminar flow in practice, by a stroke of serendipity they proved to be excellent high-speed airfoils for jet-powered airplanes after 1945. Beginning in 1965 National Aeronautics and Space Administration (NASA)

Designation	Date	Diagram
Wright	1908	
Bleriot	1909	
R.A.F. 6	1912	
R.A.F. 15	1915	
U.S.A. 27	1919	
Joukowsky (Göttingen 430)	1912	
Göttingen 398	1919	
Göttingen 387	1919	
Clark Y	1922	
M-6	1926	
R.A.F. 34	1926	
N.A.C.A. 2412	1933	
N.A.C.A. 23012	1935	
N.A.C.A. 23021	1935	

Figure 4.1 Historical sequence of airfoil sections.
(Millikan, Clark B., *Aerodynamics of the Airplane*, Wiley, 1941.)

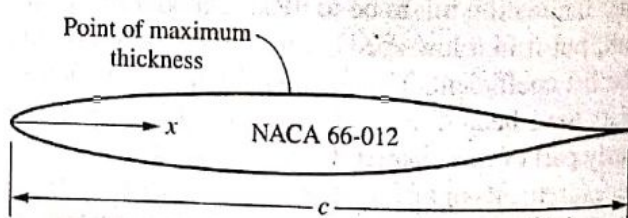


Figure 4.2 Laminar-flow airfoil shape.

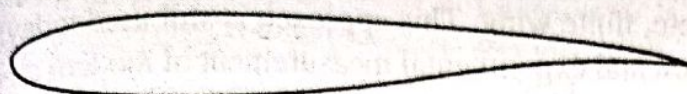


Figure 4.3 Supercritical airfoil shape.

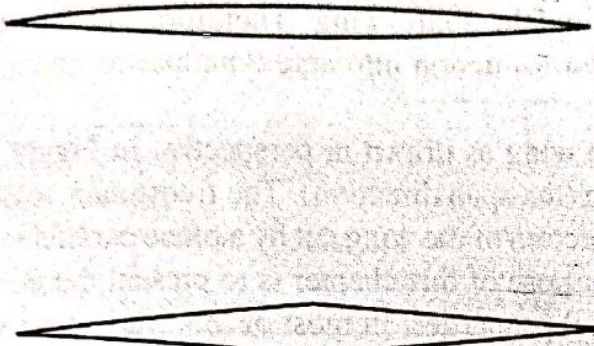


Figure 4.4 Supersonic airfoil shapes.

developed another series of revolutionary airfoil shapes, supercritical airfoils, designed for efficient flight near Mach one; a typical supercritical airfoil shape is shown in Figure 4.3. Classic airfoil shapes for supersonic flow are shown in Figure 4.4; note the very slender profiles with sharp leading edges. All the airfoil shapes shown in Figure 4.1 through 4.4 were designed for specific purposes in their time and have been used on untold numbers of different airplanes. Today, the proper design of new airfoil shapes is more important than ever. Using numerical

techniques, aircraft companies usually custom-design the airfoil shapes for new airplanes, shapes that best fit the design requirements for the specific airplane. This chapter is exclusively devoted to the study of airfoils; it discusses the fundamental aspects of airfoil aerodynamics—aspects that are the heart of airfoil design and performance.

Figure 4.5 shows an airplane in flight, sustained in the air by the aerodynamic action of its wing. Airplane wings are made up of airfoil shapes. The first step in understanding the aerodynamics of wings is to understand the aerodynamics of airfoils. Airfoil aerodynamics is important stuff—it is the stuff of this chapter. Moreover, it is truly interesting. It is fun to visualize the flow over an airfoil and to learn how to calculate the resulting lift on the airfoil. Read on and enjoy.

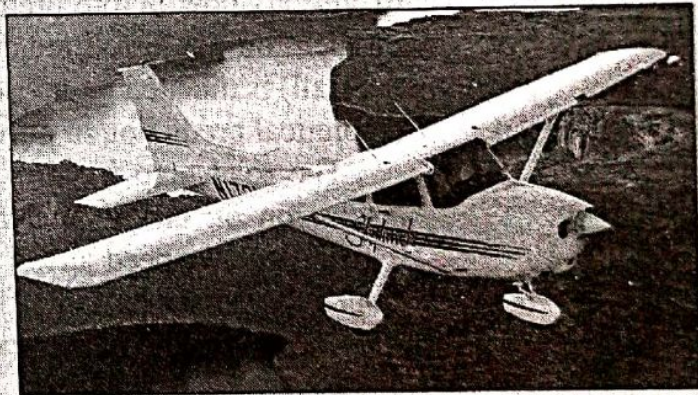


Figure 4.5 Cessna Skyhawk. (*Cessna Aircraft Co.*)

4.1 INTRODUCTION

With the advent of successful powered flight at the turn of the twentieth century, the importance of aerodynamics ballooned almost overnight. In turn, interest grew in the understanding of the aerodynamic action of such lifting surfaces as fixed wings on airplanes and, later, rotors on helicopters. In the period 1912–1918, the analysis of airplane wings took a giant step forward when Ludwig Prandtl and his colleagues at Göttingen, Germany, showed that the aerodynamic consideration of wings could be split into two parts: (1) the study of the

section of a wing—an airfoil—and (2) the modification of such airfoil properties to account for the complete, finite wing. This approach is still used today; indeed, the theoretical calculation and experimental measurement of modern airfoil properties have been a major part of the aeronautics research carried out by the National Aeronautics and Space Administration (NASA) in the 1970s and 1980s. (See Chapter 5 of Reference 2 for a historical sketch on airfoil development and Reference 10 for a description of modern airfoil research.) Following Prandtl's philosophy, the present chapter deals exclusively with airfoils, whereas Chapter 5 treats the case of a complete, finite wing. Therefore, in this chapter and Chapter 5, we make a major excursion into aerodynamics as applied to airplanes.

What is an airfoil? Consider a wing as drawn in perspective in Figure 4.6. The wing extends in the y direction (the span direction). The freestream velocity V_∞ is parallel to the xz plane. Any section of the wing cut by a plane parallel to the xz plane is called an *airfoil*. The purpose of this chapter is to present theoretical methods for the calculation of airfoil properties. In most of this chapter we will deal with inviscid flow, which does not lead to predictions of airfoil drag; indeed, d'Alembert's paradox says that the drag on an airfoil is zero—clearly not a realistic answer. We will have to wait until Section 4.12 and Chapter 15 and a discussion of viscous flow before predictions of drag can be made. However, the lift and moment on the airfoil are due mainly to the pressure distribution, which (below the stall) is dictated by inviscid flow. Therefore, this chapter concentrates on the theoretical prediction of airfoil lift and moments.

The road map for this chapter is given in Figure 4.7. After some initial discussion on airfoil nomenclature and characteristics, we present two approaches to low-speed airfoil theory. One is the classical thin airfoil theory developed during the period 1910–1920 (the right-hand branch of Figure 4.7). The other is the modern numerical approach for arbitrary airfoils using vortex panels

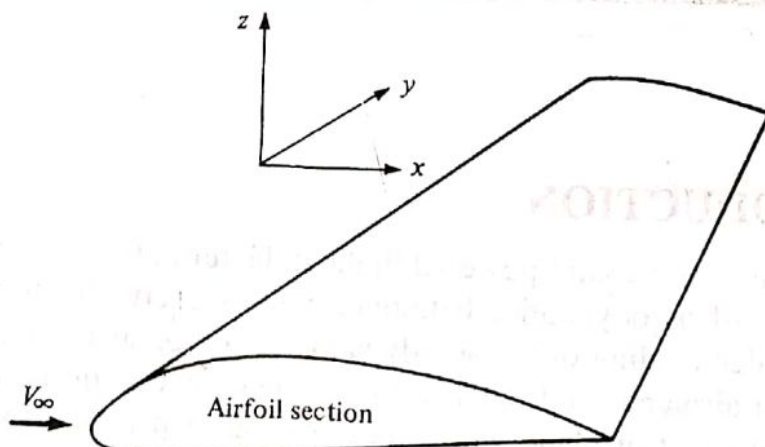


Figure 4.6 Definition of an airfoil.

(the left-hand branch of Figure 4.7). Please refer to this road map as you work your way through this chapter.

4.2 AIRFOIL NOMENCLATURE

The first patented airfoil shapes were developed by Horatio F. Phillips in 1884. Phillips was an Englishman who carried out the first serious wind-tunnel experiments on airfoils. In 1902, the Wright brothers conducted their own airfoil tests in a wind tunnel, developing relatively efficient shapes which contributed to their successful first flight on December 17, 1903 (see Section 1.1). Clearly, in the early days of powered flight, airfoil design was basically customized and personalized. However, in the early 1930s, NACA—the forerunner of NASA—embarked on a series of definitive airfoil experiments using airfoil shapes that were constructed rationally and systematically. Many of these NACA airfoils are in common use today. Therefore, in this chapter we follow the nomenclature established by the NACA; such nomenclature is now a well-known standard.

Consider the airfoil sketched in Figure 4.8. The *mean camber line* is the locus of points halfway between the upper and lower surfaces as measured perpendicular to the mean camber line itself. The most forward and rearward points of the mean camber line are the *leading and trailing edges*, respectively. The straight line connecting the leading and trailing edges is the *chord line* of the airfoil, and the precise distance from the leading to the trailing edge measured along the chord line is simply designated the *chord c* of the airfoil. The *camber* is the maximum distance between the mean camber line and the chord line, measured perpendicular to the chord line. The *thickness* is the distance between the upper and lower surfaces, also measured perpendicular to the chord line. The shape of the airfoil at the leading edge is usually circular, with a leading-edge radius of approximately $0.02c$. The shapes of all standard NACA airfoils are generated by specifying the shape of the mean camber line and then wrapping a specified symmetrical thickness distribution around the mean camber line.

The force-and-moment system on an airfoil was discussed in Section 1.5, and the relative wind, angle of attack, lift, and drag were defined in Figure 1.16. You should review these considerations before proceeding further.

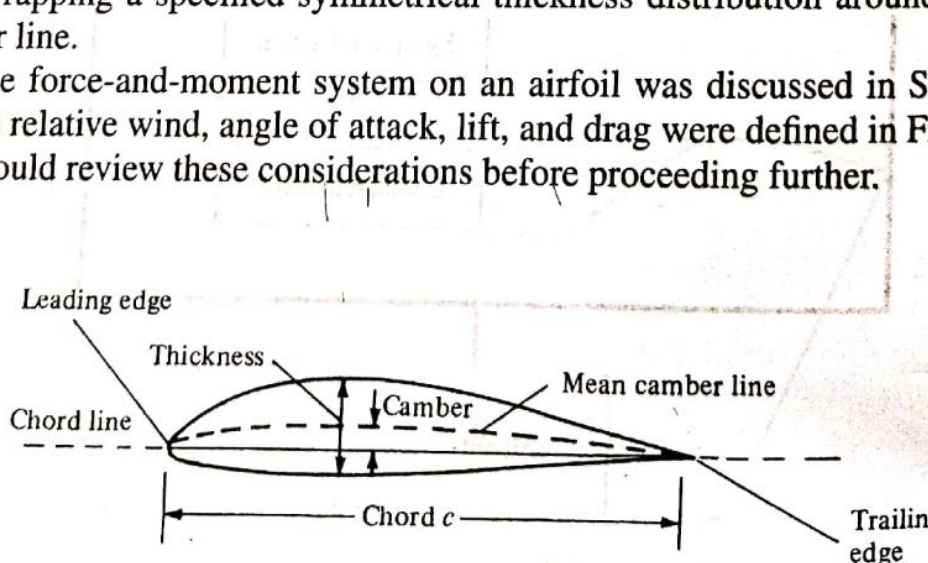


Figure 4.8 Airfoil nomenclature.

The NACA identified different airfoil shapes with a logical numbering system. For example, the first family of NACA airfoils, developed in the 1930s, was the "four-digit" series, such as the NACA 2412 airfoil. Here, the first digit is the maximum camber in hundredths of chord, the second digit is the location of maximum camber along the chord from the leading edge in tenths of chord, and the last two digits give the maximum thickness in hundredths of chord. For the NACA 2412 airfoil, the maximum camber is $0.02c$ located at $0.4c$ from the leading edge, and the maximum thickness is $0.12c$. It is common practice to state these numbers in percent of chord, that is, 2 percent camber at 40 percent chord, with 12 percent thickness. An airfoil with no camber, that is, with the camber line and chord line coincident, is called a *symmetric airfoil*. Clearly, the shape of a symmetric airfoil is the same above and below the chord line. For example, the NACA 0012 airfoil is a symmetric airfoil with a maximum thickness of 12 percent.

The second family of NACA airfoils was the "five-digit" series, such as the NACA 23012 airfoil. Here, the first digit when multiplied by $\frac{3}{2}$ gives the design lift coefficient¹ in tenths, the next two digits when divided by 2 give the location of maximum camber along the chord from the leading edge in hundredths of chord, and the final two digits give the maximum thickness in hundredths of chord. For the NACA 23012 airfoil, the design lift coefficient is 0.3, the location of maximum camber is at $0.15c$, and the airfoil has 12 percent maximum thickness.

One of the most widely used family of NACA airfoils is the "6-series" laminar flow airfoils, developed during World War II. An example is the NACA 65-218. Here, the first digit simply identifies the series, the second gives the location of minimum pressure in tenths of chord from the leading edge (for the basic symmetric thickness distribution at zero lift), the third digit is the design lift coefficient in tenths, and the last two digits give the maximum thickness in hundredths of chord. For the NACA 65-218 airfoil, the 6 is the series designation, the minimum pressure occurs at $0.5c$ for the basic symmetric thickness distribution at zero lift, the design lift coefficient is 0.2, and the airfoil is 18 percent thick.

The complete NACA airfoil numbering system is given in Reference 11. Indeed, Reference 11 is a definitive presentation of the classic NACA airfoil work up to 1949. It contains a discussion of airfoil theory, its application, coordinates for the shape of NACA airfoils, and a huge bulk of experimental data for these airfoils. This author strongly encourages you to read Reference 11 for a thorough presentation of airfoil characteristics.

As a matter of interest, the following is a short partial listing of airplanes currently in service that use standard NACA airfoils.

¹ The design lift coefficient is the theoretical lift coefficient for the airfoil when the angle of attack is such that the slope of the mean camber line at the leading edge is parallel to the freestream velocity.

Airplane	Airfoil
Beechcraft Sundowner	NACA 63A415
Beechcraft Bonanza	NACA 23016.5 (at root) NACA 23012 (at tip)
Cessna 150	NACA 2412
Fairchild A-10	NACA 6716 (at root) NACA 6713 (at tip)
Gates Learjet 24D	NACA 64A109
General Dynamics F-16	NACA 64A204
Lockheed C-5 Galaxy	NACA 0012 (modified)

In addition, many of the large aircraft companies today design their own special-purpose airfoils; for example, the Boeing 727, 737, 747, 757, 767, and 777 all have specially designed Boeing airfoils. Such capability is made possible by modern airfoil design computer programs utilizing either panel techniques or direct numerical finite-difference solutions of the governing partial differential equations for the flow field. (Such equations are developed in Chapter 2.)

4.3 AIRFOIL CHARACTERISTICS

Before discussing the theoretical calculation of airfoil properties, let us examine some typical results. During the 1930s and 1940s, the NACA carried out numerous measurements of the lift, drag, and moment coefficients on the standard NACA airfoils. These experiments were performed at low speeds in a wind tunnel where the constant-chord wing spanned the entire test section from one sidewall to the other. In this fashion, the flow "sees" a wing without wing tips—a so-called infinite wing, which theoretically stretches to infinity along the span (in the y direction in Figure 4.6). Because the airfoil section is the same at any spanwise location along the infinite wing, the properties of the airfoil and the infinite wing are identical. Hence, airfoil data are frequently called infinite wing data. (In contrast, we see in Chapter 5 that the properties of a finite wing are somewhat different from its airfoil properties.)

The typical variation of lift coefficient with angle of attack for an airfoil is sketched in Figure 4.9. At low-to-moderate angles of attack, c_l varies linearly with α ; the slope of this straight line is denoted by a_0 and is called the *lift slope*. In this region, the flow moves smoothly over the airfoil and is attached over most of the surface, as shown in the streamline picture at the left of Figure 4.9. However, as α becomes large, the flow tends to separate from the top surface of the airfoil, creating a large wake of relatively "dead air" behind the airfoil as shown at the right of Figure 4.9. Inside this separated region, the flow is recirculating, and part of the flow is actually moving in a direction opposite to the freestream—so-called reversed flow. (Refer also to Figure 1.42.) This separated flow is due to viscous effects and is discussed in Section 4.12 and Chapter 15. The consequence of this separated flow at high α is a precipitous decrease in lift and a large increase in drag; under such conditions the airfoil is said to be *stalled*. The maximum

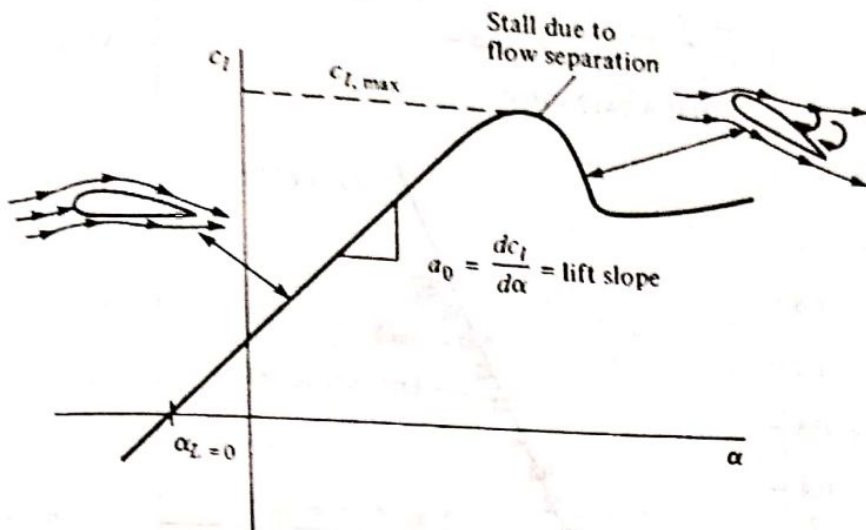


Figure 4.9 Schematic of lift-coefficient variation with angle of attack for an airfoil.

value of c_l , which occurs just prior to the stall, is denoted by $c_{l,\max}$; it is one of the most important aspects of airfoil performance, because it determines the stalling speed of an airplane. The higher is $c_{l,\max}$, the lower is the stalling speed. A great deal of modern airfoil research has been directed toward increasing $c_{l,\max}$. Again examining Figure 4.9, we see that c_l increases linearly with α until flow separation begins to have an effect. Then the curve becomes nonlinear, c_l reaches a maximum value, and finally the airfoil stalls. At the other extreme of the curve, noting Figure 4.9, the lift at $\alpha = 0$ is finite; indeed, the lift goes to zero only when the airfoil is pitched to some negative angle of attack. The value of α when lift equals zero is called the *zero-lift angle of attack* and is denoted by $\alpha_{L=0}$. For a symmetric airfoil, $\alpha_{L=0} = 0$, whereas for all airfoils with positive camber (camber *above* the chord line), $\alpha_{L=0}$ is a negative value, usually on the order of -2 or -3° .

The inviscid flow airfoil theory discussed in this chapter allows us to predict the lift slope a_0 and $\alpha_{L=0}$ for a given airfoil. It does not allow us to calculate $c_{l,\max}$, which is a difficult viscous flow problem, to be discussed in Chapters 15 to 20.

Experimental results for lift and moment coefficients for the NACA 2412 airfoil are given in Figure 4.10. Here, the moment coefficient is taken about the quarter-chord point. Recall from Section 1.6 that the force-and-moment system on an airfoil can be transferred to any convenient point; however, the quarter-chord point is commonly used. (Refresh your mind on this concept by reviewing Section 1.6, especially Figure 1.25.) Also shown in Figure 4.10 are theoretical results to be discussed later. Note that the experimental data are given for two different Reynolds numbers. The lift slope a_0 is not influenced by Re ; however, $c_{l,\max}$ is dependent upon Re . This makes sense, because $c_{l,\max}$ is governed by viscous effects, and Re is a similarity parameter that governs the strength of inertia forces relative to viscous forces in the flow. [See Section 1.7 and Equation (1.35).]

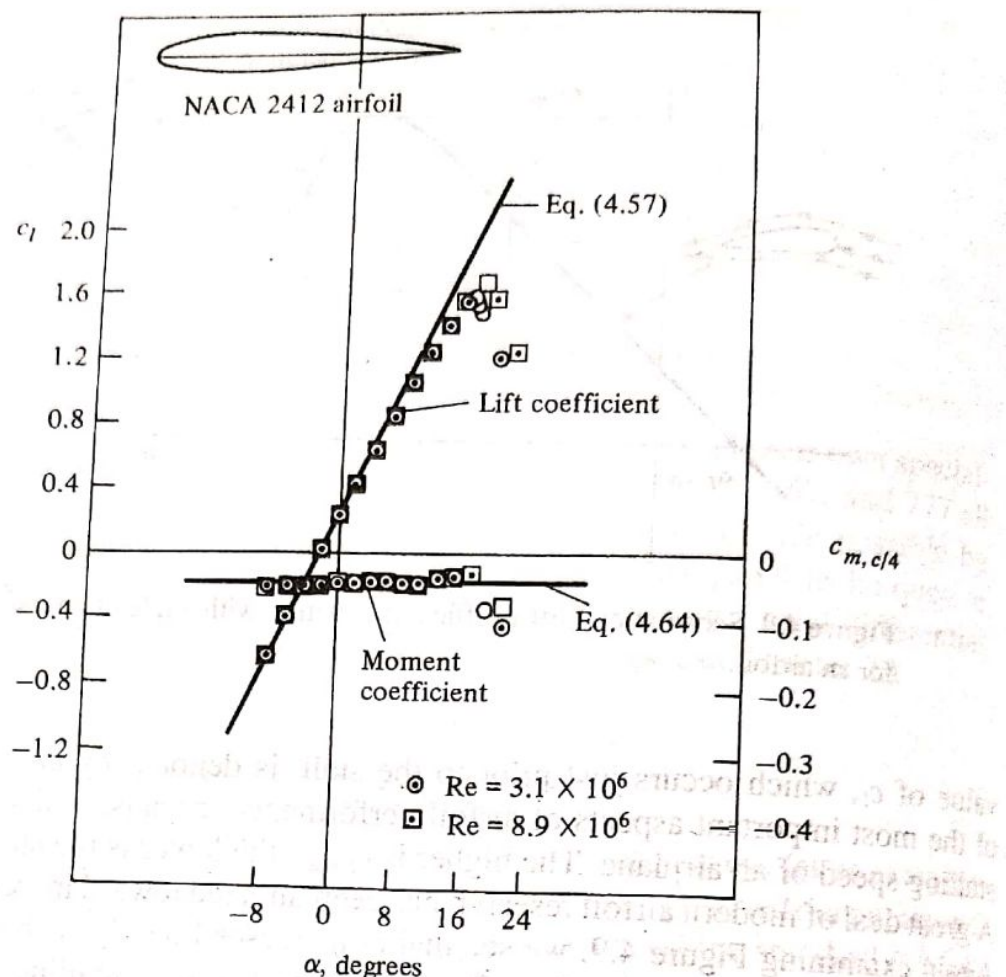


Figure 4.10 Experimental data for lift coefficient and moment coefficient about the quarter-chord point for an NACA 2412 airfoil.
 (Source: Data obtained from Abbott and von Doenhoff, Reference 11.)
 Also shown is a comparison with theory described in Section 4.8.

The moment coefficient is also insensitive to Re except at large α . The NACA 2412 airfoil is a commonly used airfoil, and the results given in Figure 4.10 are quite typical of airfoil characteristics. For example, note from Figure 4.10 that $\alpha_{L=0} = -2.1^\circ$, $c_{L,\max} \approx 1.6$, and the stall occurs at $\alpha \approx 16^\circ$.

This chapter deals primarily with airfoil theory for an inviscid, incompressible flow; such theory is incapable of predicting airfoil drag, as noted earlier. However, for the sake of completeness, experimental data for the drag coefficient c_d for the NACA 2412 airfoil are given in Figure 4.11 as a function of the angle of attack.² The physical source of this drag coefficient is both skin friction drag and pressure drag due to flow separation (so-called form drag). The sum of these two

² In many references, such as Reference 11, it is common to plot c_d versus c_L , rather than versus α . A plot of c_d versus c_L is called a *drag polar*. For the sake of consistency with Figure 4.10, we choose to plot c_d versus α here.

From Figures 4.10 and 4.11, we have

α	C_l	C_d	C_l/C_d
0	0.25	0.0065	38.5
4	0.65	0.0070	93
8	1.08	0.0112	96
12	1.44	0.017	85

Note that, as the angle of attack increases, the lift-to-drag ratio first increases, reaches a maximum, and then decreases. The maximum lift-to-drag ratio, $(L/D)_{\max}$, is an important parameter in airfoil performance; it is a direct measure of aerodynamic efficiency. The higher the value of $(L/D)_{\max}$, the more efficient is the airfoil. The values of L/D for airfoils are quite large numbers in comparison to that for a complete airplane. Due to the extra drag associated with all parts of the airplane, values of $(L/D)_{\max}$ for real airplanes are on the order of 10 to 20.

4.4 PHILOSOPHY OF THEORETICAL SOLUTIONS FOR LOW-SPEED FLOW OVER AIRFOILS: THE VORTEX SHEET

In Section 3.14, the concept of vortex flow was introduced; refer to Figure 3.31 for a schematic of the flow induced by a point vortex of strength Γ located at a given point O . (Recall that Figure 3.31, with its counterclockwise flow, corresponds to a negative value of Γ . By convention, a positive Γ induces a clockwise flow.) Let us now expand our concept of a point vortex. Referring to Figure 3.31, imagine a straight line perpendicular to the page, going through point O , and extending to infinity both out of and into the page. This line is a straight *vortex filament* of strength Γ . A straight vortex filament is drawn in perspective in Figure 4.12. (Here, we show a clockwise flow, which corresponds to a positive value of Γ .) The flow induced in any plane perpendicular to the straight vortex filament by the filament itself is identical to that induced by a point vortex of strength Γ ; that is, in Figure 4.12, the flows in the planes perpendicular to the vortex filament at O and O' are identical to each other and are identical to the flow induced by a point vortex of strength Γ . Indeed, the point vortex described in Section 3.14 is simply a section of a straight vortex filament.

In Section 3.17, we introduced the concept of a source sheet, which is an infinite number of line sources side by side, with the strength of each line source being infinitesimally small. For vortex flow, consider an analogous situation. Imagine an infinite number of straight vortex filaments side by side, where the strength of each filament is infinitesimally small. These side-by-side vortex filaments form a *vortex sheet*, as shown in perspective in the upper left of Figure 4.13. If we look along the series of vortex filaments (looking along the y axis in Figure 4.13), the vortex sheet will appear as sketched at the lower right of Figure 4.13. Here, we are looking at an edge view of the sheet; the vortex filaments are all perpendicular

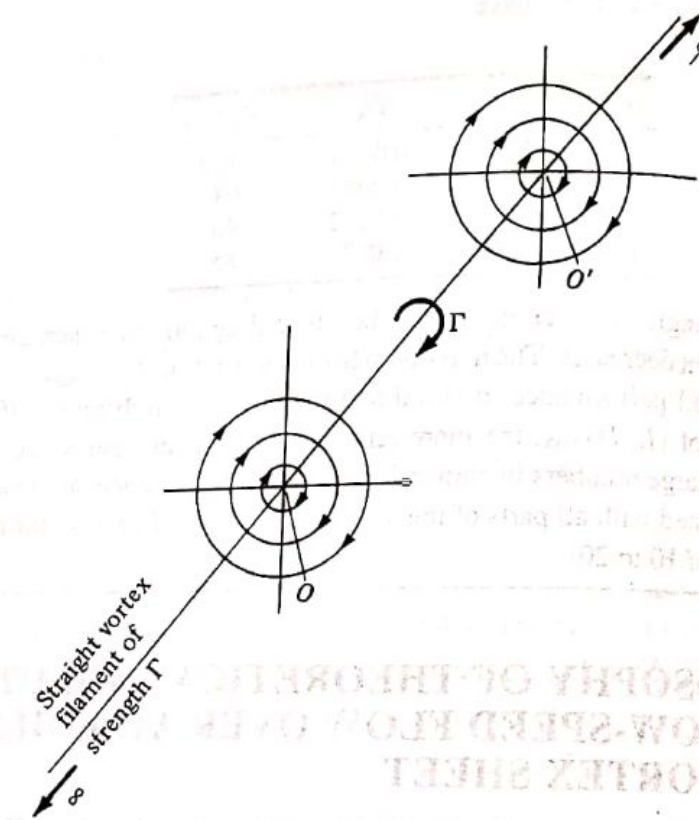


Figure 4.12 Vortex filament.

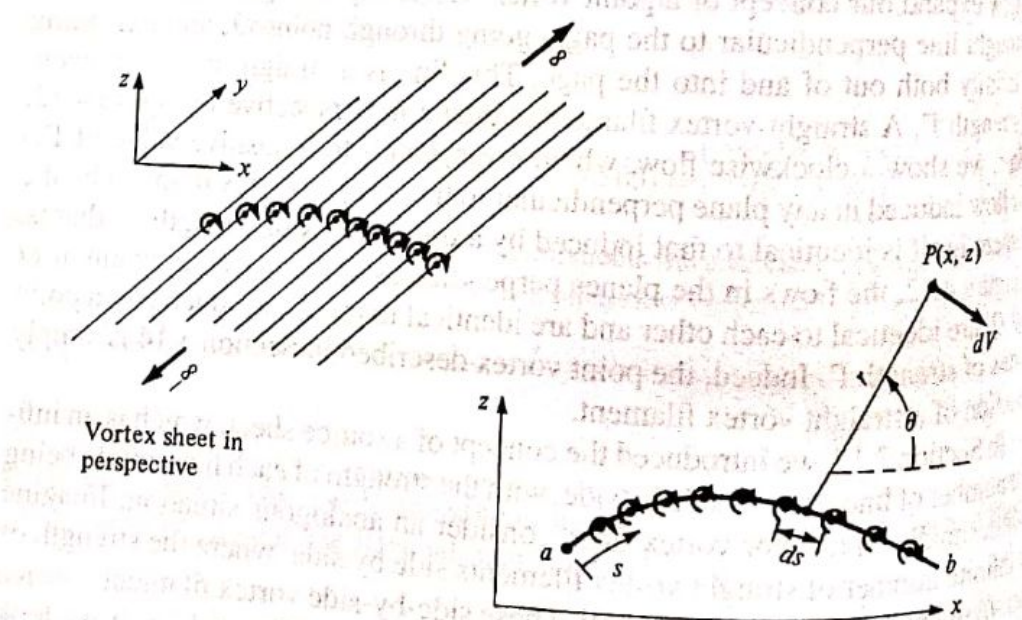


Figure 4.13 Vortex sheet.

to the page. Let s be the distance measured along the vortex sheet in the edge view. Define $\gamma = \gamma(s)$ as the strength of the vortex sheet, per unit length along s . Thus, the strength of an infinitesimal portion ds of the sheet is γds . This small section of the vortex sheet can be treated as a distinct vortex of strength γds . Now consider point P in the flow, located a distance r from ds ; the Cartesian coordinates of P are (x, z) . The small section of the vortex sheet of strength γds , induces an infinitesimally small velocity dV at point P . From Equation (3.105), dV is given by

$$dV = -\frac{\gamma ds}{2\pi r} \quad (4.1)$$

and is in a direction perpendicular to r , as shown in Figure 4.13. The velocity at P induced by the entire vortex sheet is the summation of Equation (4.1) from point a to point b . Note that dV , which is perpendicular to r , changes direction at point P as we sum from a to b ; hence, the incremental velocities induced at P by different sections of the vortex sheet must be added vectorially. Because of this, it is sometimes more convenient to deal with the velocity potential. Again referring to Figure 4.13, the increment in velocity potential $d\phi$ induced at point P by the elemental vortex γds is, from Equation (3.112),

$$d\phi = -\frac{\gamma ds}{2\pi} \theta \quad (4.2)$$

In turn, the velocity potential at P due to the entire vortex sheet from a to b is

$$\phi(x, z) = -\frac{1}{2\pi} \int_a^b \theta \gamma ds \quad (4.3)$$

Equation (4.1) is particularly useful for our discussion of classical thin airfoil theory, whereas Equation (4.3) is important for the numerical vortex panel method.

Recall from Section 3.14 that the circulation Γ around a point vortex is equal to the strength of the vortex. Similarly, the circulation around the vortex sheet in Figure 4.13 is the sum of the strengths of the elemental vortices; that is

$$\Gamma = \int_a^b \gamma ds \quad (4.4)$$

Recall that the source sheet introduced in Section 3.17 has a discontinuous change in the direction of the *normal* component of velocity across the sheet (from Figure 3.38, note that the normal component of velocity changes direction by 180° in crossing the sheet), whereas the tangential component of velocity is the same immediately above and below the source sheet. In contrast, for a vortex sheet, there is a discontinuous change in the tangential component of velocity across the sheet, whereas the normal component of velocity is preserved across the sheet. This change in tangential velocity across the vortex sheet is related to the strength of the sheet as follows. Consider a vortex sheet as sketched in

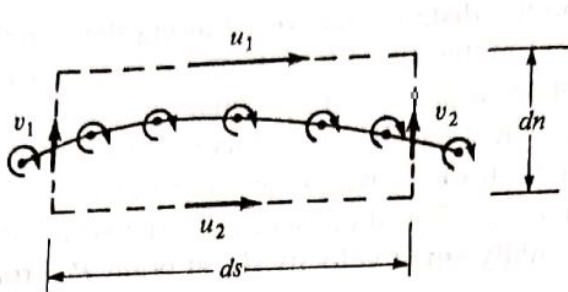


Figure 4.14 Tangential velocity jump across a vortex sheet.

Figure 4.14. Consider the rectangular dashed path enclosing a section of the sheet of length ds . The velocity components tangential to the top and bottom of this rectangular path are u_1 and u_2 , respectively, and the velocity components tangential to the left and right sides are v_1 and v_2 , respectively. The top and bottom of the path are separated by the distance dn . From the definition of circulation given by Equation (2.36), the circulation around the dashed path is

$$\Gamma = -(v_2 dn - u_1 ds - v_1 dn + u_2 ds)$$

or

$$\Gamma = (u_1 - u_2) ds + (v_1 - v_2) dn \quad (4.5)$$

However, since the strength of the vortex sheet contained inside the dashed path is γds , we also have

$$\Gamma = \gamma ds \quad (4.6)$$

Therefore, from Equations (4.5) and (4.6),

$$\gamma ds = (u_1 - u_2) ds + (v_1 - v_2) dn \quad (4.7)$$

Let the top and bottom of the dashed line approach the vortex sheet; that is, let $dn \rightarrow 0$. In the limit, u_1 and u_2 become the velocity components tangential to the vortex sheet immediately above and below the sheet, respectively, and Equation (4.7) becomes

$$\gamma ds = (u_1 - u_2) ds$$

or

$$\boxed{\gamma = u_1 - u_2} \quad (4.8)$$

Equation (4.8) is important; it states that *the local jump in tangential velocity across the vortex sheet is equal to the local sheet strength*.

We have now defined and discussed the properties of a vortex sheet. The concept of a vortex sheet is instrumental in the analysis of the low-speed characteristics of an airfoil. A philosophy of airfoil theory of inviscid, incompressible flow is as follows. Consider an airfoil of arbitrary shape and thickness in a freestream with velocity V_∞ , as sketched in Figure 4.15. Replace the airfoil surface with a vortex sheet of variable strength $\gamma(s)$, as also shown in Figure 4.15. Calculate the variation of γ as a function of s such that the induced velocity field from the vortex sheet when added to the uniform velocity of magnitude V_∞ will make

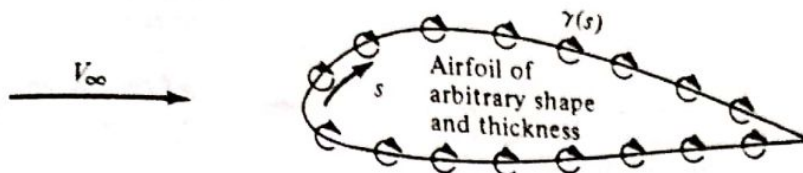


Figure 4.15 Simulation of an arbitrary airfoil by distributing a vortex sheet over the airfoil surface.

the vortex sheet (hence the airfoil surface) a *streamline of the flow*. In turn, the circulation around the airfoil will be given by

$$\Gamma = \int \gamma ds$$

where the integral is taken around the complete surface of the airfoil. Finally, the resulting lift is given by the Kutta-Joukowski theorem:

$$L' = \rho_\infty V_\infty \Gamma$$

This philosophy is not new. It was first espoused by Ludwig Prandtl and his colleagues at Göttingen, Germany, during the period 1912–1922. However, no general analytical solution for $\gamma = \gamma(s)$ exists for an airfoil of arbitrary shape and thickness. Rather, the strength of the vortex sheet must be found numerically, and the practical implementation of the above philosophy had to wait until the 1960s with the advent of large digital computers. Today, the above philosophy is the foundation of the modern vortex panel method, to be discussed in Section 4.9.

The concept of replacing the airfoil surface in Figure 4.15 with a vortex sheet is more than just a mathematical device; it also has physical significance. In real life, there is a thin boundary layer on the surface, due to the action of friction between the surface and the airflow (see Figures 1.41 and 1.46). This boundary layer is a highly viscous region in which the large velocity gradients produce substantial vorticity; that is, $\nabla \times \mathbf{V}$ is finite within the boundary layer. (Review Section 2.12 for a discussion of vorticity.) Hence, in real life, there is a distribution of vorticity along the airfoil surface due to viscous effects, and our philosophy of replacing the airfoil surface with a vortex sheet (such as in Figure 4.15) can be construed as a way of modeling this effect in an inviscid flow.³

Imagine that the airfoil in Figure 4.15 is made very thin. If you were to stand back and look at such a thin airfoil from a distance, the portions of the vortex sheet

³ It is interesting to note that some recent research by NASA is hinting that even as complex a problem as flow separation, heretofore thought to be a completely viscous-dominated phenomenon, may in reality be an inviscid-dominated flow which requires only a rotational flow. For example, some inviscid flow-field numerical solutions for flow over a circular cylinder, when vorticity is introduced either by means of a nonuniform freestream or a curved shock wave, are accurately predicting the separated flow on the rearward side of the cylinder. However, as exciting as these results may be, they are too preliminary to be emphasized in this book. We continue to talk about flow separation in Chapters 15 to 20 as being a viscous-dominated effect, until definitely proved otherwise. This recent research is mentioned here only as another example of the physical connection between vorticity, vortex sheets, viscosity, and real life.

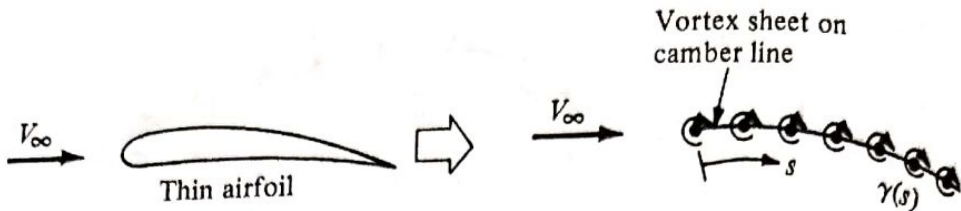


Figure 4.16 Thin airfoil approximation.

on the top and bottom surface of the airfoil would almost coincide. This gives rise to a method of approximating a thin airfoil by replacing it with a single vortex sheet distributed over the camber line of the airfoil, as sketched in Figure 4.16. The strength of this vortex sheet $\gamma(s)$ is calculated such that, in combination with the freestream, the camber line becomes a streamline of the flow. Although the approach shown in Figure 4.16 is approximate in comparison with the case shown in Figure 4.15, it has the advantage of yielding a closed-form analytical solution. This philosophy of thin airfoil theory was first developed by Max Munk, a colleague of Prandtl, in 1922 (see Reference 12). It is discussed in Sections 4.7 and 4.8.

4.5 THE KUTTA CONDITION

The lifting flow over a circular cylinder was discussed in Section 3.15, where we observed that an infinite number of potential flow solutions were possible, corresponding to the infinite choice of Γ . For example, Figure 3.28 illustrates three different flows over the cylinder, corresponding to three different values of Γ . The same situation applies to the potential flow over an airfoil; for a given airfoil at a given angle of attack, there are an infinite number of valid theoretical solutions, corresponding to an infinite choice of Γ . For example, Figure 4.17 illustrates two different flows over the same airfoil at the same angle of attack but with different values of Γ . At first, this may seem to pose a dilemma. We know from experience that a given airfoil at a given angle of attack produces a single value of lift (e.g., see Figure 4.10). So, although there is an infinite number of possible potential flow solutions, nature knows how to pick a particular solution. Clearly, the philosophy discussed in the previous section is not complete—we need an additional condition that fixes Γ for a given airfoil at a given α .

To attempt to find this condition, let us examine some experimental results for the development of the flow field around an airfoil which is set into motion from an initial state of rest. Figure 4.18 shows a series of classic photographs of the flow over an airfoil, taken from Prandtl and Tietjens (Reference 8). In Figure 4.18a, the flow has just started, and the flow pattern is just beginning to develop around the airfoil. In these early moments of development, the flow tries to curl around the sharp trailing edge from the bottom surface to the top surface, similar to the sketch shown at the left of Figure 4.17. However, more advanced considerations of inviscid, incompressible flow (see, e.g., Reference 9) show the theoretical result that the velocity becomes infinitely large at a sharp corner. Hence, the type

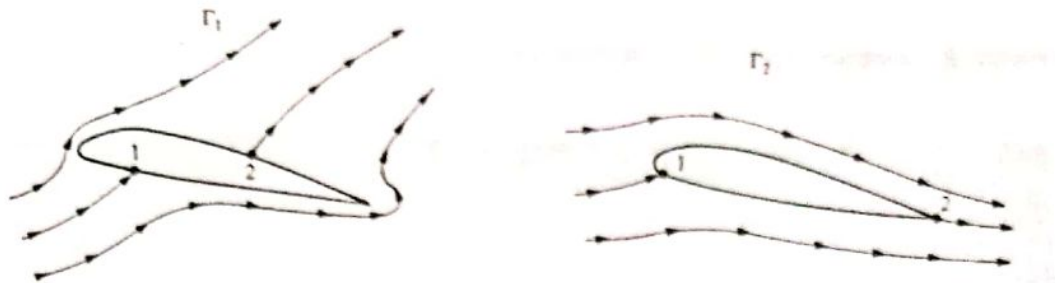
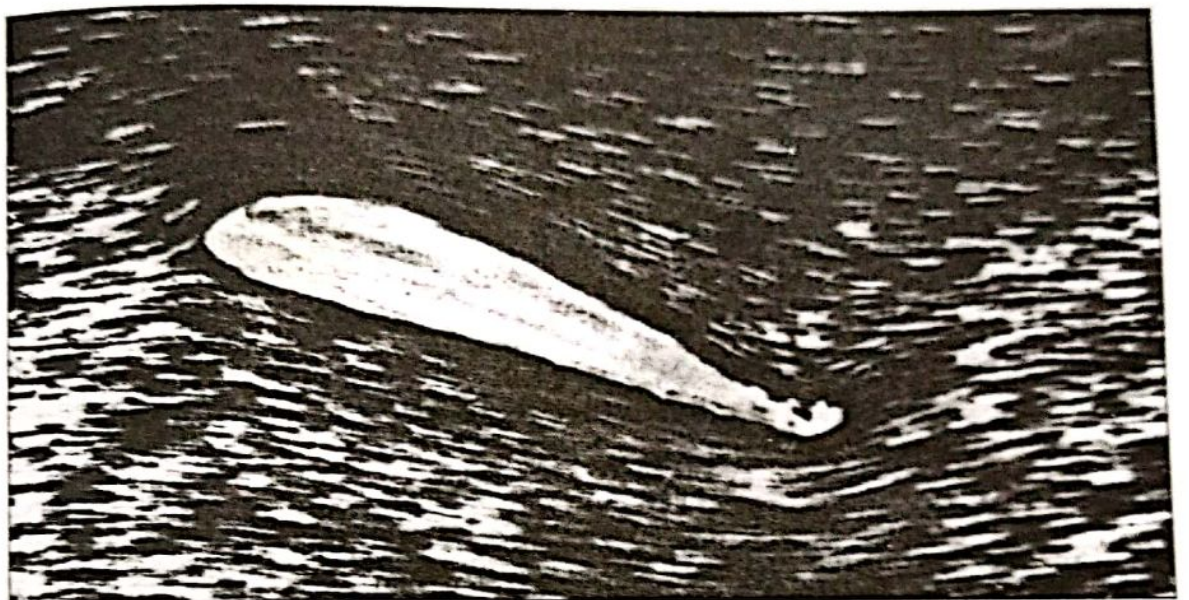
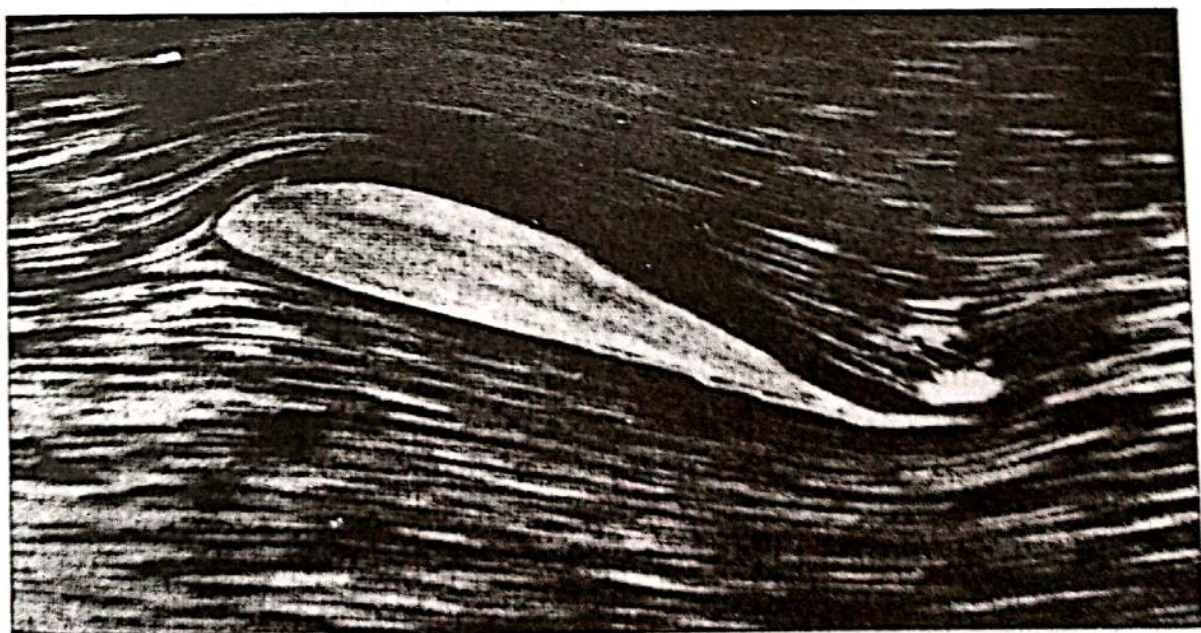


Figure 4.17 Effect of different values of circulation on the potential flow over a given airfoil at a given angle of attack. Points 1 and 2 are stagnation points.

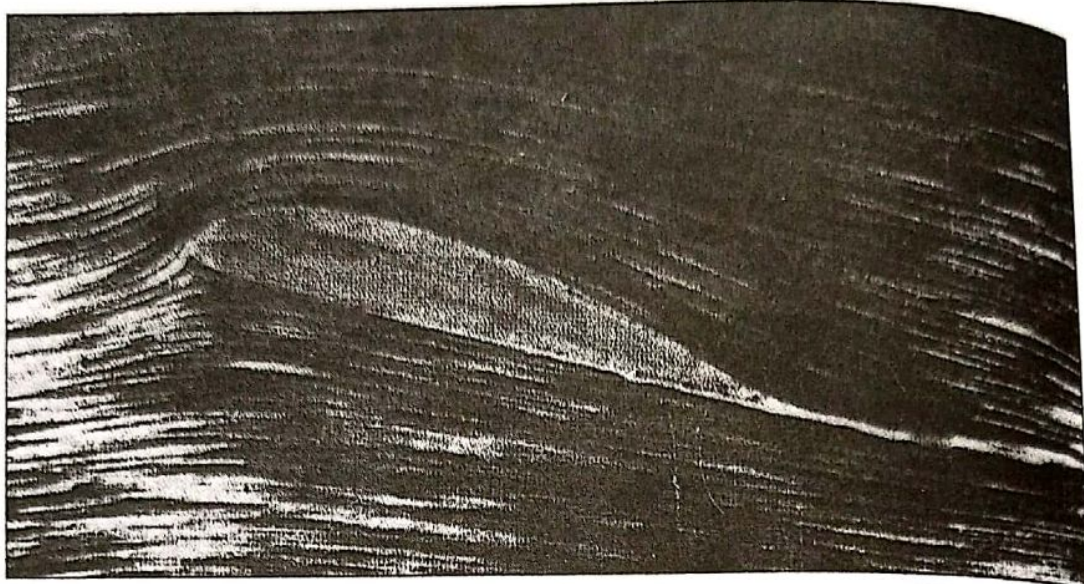


(a)



(b)

Figure 4.18 The development of steady flow over an airfoil; the airfoil is impulsively started from rest and attains a steady velocity through the fluid. (a) A moment just after starting. (b) An intermediate time. (Source: Prandtl and Tijens, Reference 8.)



(c)

Figure 4.18 (continued) The development of steady flow over an airfoil; the airfoil is impulsively started from rest and attains a steady velocity through the fluid. (c) The final steady flow. (*Source: Prandtl and Tijens, Reference 8.*)

of flow sketched at the left of Figure 4.17, and shown in Figure 4.18a, is not tolerated very long by nature. Rather, as the real flow develops over the airfoil, the stagnation point on the upper surface (point 2 in Figure 4.17) moves toward the trailing edge. Figure 4.18b shows this intermediate stage. Finally, after the initial transient process dies out, the steady flow shown in Figure 4.18c is reached. This photograph demonstrates that the flow is *smoothly leaving the top and the bottom surfaces of the airfoil at the trailing edge*. This flow pattern is sketched at the right of Figure 4.17 and represents the type of pattern to be expected for the steady flow over an airfoil.

Reflecting on Figures 4.17 and 4.18, we emphasize again that in establishing the steady flow over a given airfoil at a given angle of attack, nature adopts that particular value of circulation (Γ_2 in Figure 4.17) which results in the flow leaving smoothly at the trailing edge. This observation was first made and used in a theoretical analysis by the German mathematician M. Wilhelm Kutta in 1902. Therefore, it has become known as the *Kutta condition*.

In order to apply the Kutta condition in a theoretical analysis, we need to be more precise about the nature of the flow at the trailing edge. The trailing edge can have a finite angle, as shown in Figures 4.17 and 4.18 and as sketched at the left of Figure 4.19, or it can be cusped, as shown at the right of Figure 4.19. First, consider the trailing edge with a finite angle, as shown at the left of Figure 4.19. Denote the velocities along the top surface and the bottom surface as V_1 and V_2 , respectively. V_1 is parallel to the top surface at point a , and V_2 is parallel to the bottom surface at point a . For the finite-angle trailing edge, if these velocities were finite at point a , then we would have two velocities in two different directions at

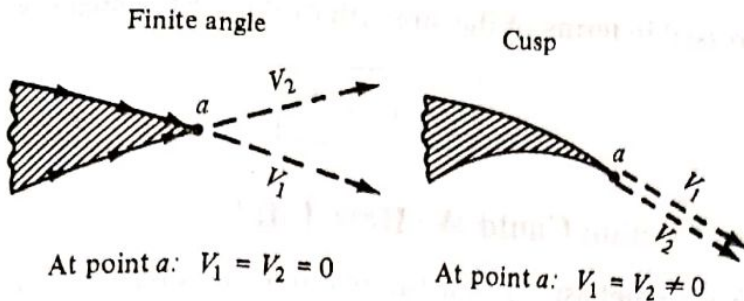


Figure 4.19 Different possible shapes of the trailing edge and their relation to the Kutta condition.

the same point, as shown at the left of Figure 4.19. However, this is not physically possible, and the only recourse is for both V_1 and V_2 to be zero at point a . That is, for the finite trailing edge, point a is a stagnation point, where $V_1 = V_2 = 0$. In contrast, for the cusped trailing edge shown at the right of Figure 4.19, V_1 and V_2 are in the same direction at point a , and hence both V_1 and V_2 can be finite. However, the pressure at point a , p_a , is a single, unique value, and Bernoulli's equation applied at both the top and bottom surfaces immediately adjacent to point a yields

$$p_a + \frac{1}{2} \rho V_1^2 = p_a + \frac{1}{2} \rho V_2^2$$

$$V_1 = V_2$$

or

Hence, for the cusped trailing edge, we see that the velocities leaving the top and bottom surfaces of the airfoil at the trailing edge are finite and equal in magnitude and direction.

We can summarize the statement of the Kutta condition as follows:

1. For a given airfoil at a given angle of attack, the value of Γ around the airfoil is such that the flow leaves the trailing edge smoothly.
2. If the trailing-edge angle is finite, then the trailing edge is a stagnation point.
3. If the trailing edge is cusped, then the velocities leaving the top and bottom surfaces at the trailing edge are finite and equal in magnitude and direction.

Consider again the philosophy of simulating the airfoil with vortex sheets placed either on the surface or on the camber line, as discussed in Section 4.4. The strength of such a vortex sheet is variable along the sheet and is denoted by $\gamma(s)$. The statement of the Kutta condition in terms of the vortex sheet is as follows. At the trailing edge (TE), from Equation (4.8), we have

$$\gamma(\text{TE}) = \gamma(a) = V_1 - V_2 \quad (4.9)$$

However, for the finite-angle trailing edge, $V_1 = V_2 = 0$; hence, from Equation (4.9), $\gamma(\text{TE}) = 0$. For the cusped trailing edge, $V_1 = V_2 \neq 0$; hence, from Equation (4.9), we again obtain the result that $\gamma(\text{TE}) = 0$. Therefore, the Kutta

condition expressed in terms of the strength of the vortex sheet is

$$\gamma(\text{TE}) = 0$$

(4.10)

4.5.1 Without Friction Could We Have Lift?

In Section 1.5 we emphasized that the resultant aerodynamic force on a body immersed in a flow is due to the net integrated effect of the pressure and shear stress distributions over the body surface. Moreover, in Section 4.1 we noted that lift on an airfoil is primarily due to the surface pressure distribution, and that shear stress has virtually no effect on lift. It is easy to see why. Look at the airfoil shapes in Figures 4.17 and 4.18, for example. Recall that pressure acts *normal* to the surface, and for these airfoils the direction of this normal pressure is essentially in the vertical direction, that is, the lift direction. In contrast the shear stress acts *tangential* to the surface, and for these airfoils the direction of this tangential shear stress is mainly in the horizontal direction, that is, the drag direction. Hence, pressure is the dominant player in the generation of lift, and shear stress has a negligible effect on lift. It is for this reason that the lift on an airfoil below the stall can be accurately predicted by *inviscid* theories such as that discussed in this chapter.

However, if we lived in a perfectly inviscid world, an airfoil could not produce lift. Indeed, the presence of friction is the very reason why we have lift. These sound like strange, even contradictory statements to our discussion in the preceding paragraph. What is going on here? The answer is that in real life, the way that nature insures that the flow will leave smoothly at the trailing edge, that is, the mechanism that nature uses to choose the flow shown in Figure 4.18c, is that the viscous boundary layer remains attached to the surface all the way to the trailing edge. *Nature enforces the Kutta condition by means of friction.* If there were no boundary layer (i.e., no friction), there would be no physical mechanism in the real world to achieve the Kutta condition.

So we are led to the most ironic situation that lift, which is created by the surface pressure distribution—an inviscid phenomenon, would not exist in a frictionless (inviscid) world. In this regard, we can say that without friction we could not have lift. However, we say this in the informed manner as discussed above.

4.6 KELVIN'S CIRCULATION THEOREM AND THE STARTING VORTEX

In this section, we put the finishing touch to the overall philosophy of airfoil theory before developing the quantitative aspects of the theory itself in subsequent sections. This section also ties up a loose end introduced by the Kutta condition described in the previous section. Specifically, the Kutta condition states that the circulation around an airfoil is just the right value to ensure that the flow smoothly leaves the trailing edge. *Question:* How does nature generate this circulation?

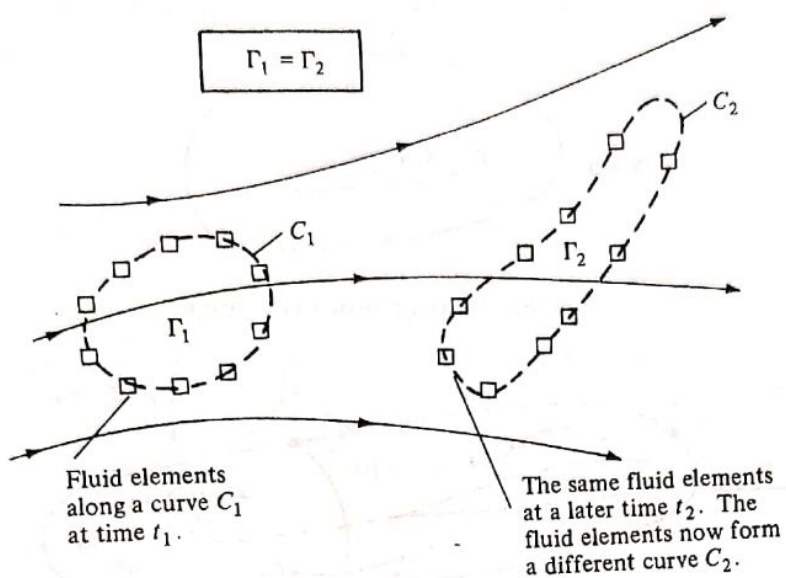


Figure 4.20 Kelvin's theorem.

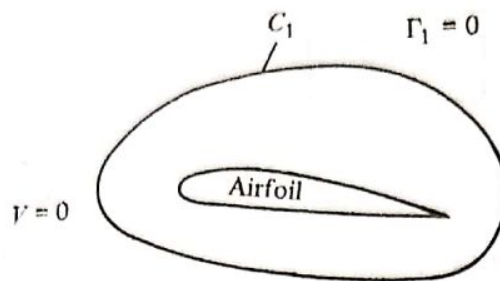
Does it come from nowhere, or is circulation somehow conserved over the whole flow field? Let us examine these matters more closely.

Consider an arbitrary inviscid, incompressible flow as sketched in Figure 4.20. Assume that all body forces \mathbf{f} are zero. Choose an arbitrary curve C_1 and identify the fluid elements that are on this curve at a given instant in time t_1 . Also, by definition the circulation around curve C_1 is $\Gamma_1 = - \int_{C_1} \mathbf{V} \cdot d\mathbf{s}$. Now let these specific fluid elements move downstream. At some later time, t_2 , these same fluid elements will form another curve C_2 , around which the circulation is $\Gamma_2 = - \int_{C_2} \mathbf{V} \cdot d\mathbf{s}$. For the conditions stated above, we can readily show that $\Gamma_1 = \Gamma_2$. In fact, since we are following a set of specific fluid elements, we can state that circulation around a closed curve formed by a set of contiguous fluid elements remains constant as the fluid elements move throughout the flow. Recall from Section 2.9 that the substantial derivative gives the time rate of change following a given fluid element. Hence, a mathematical statement of the above discussion is simply

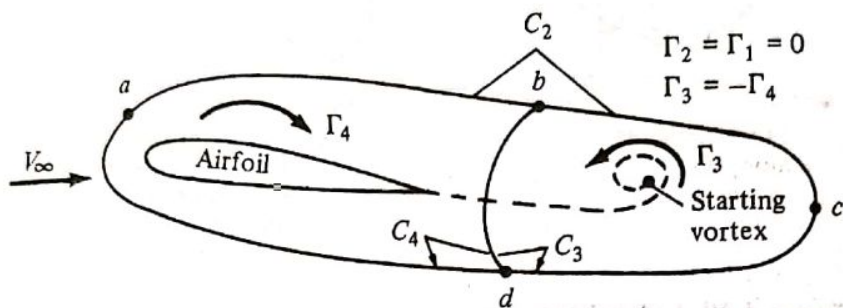
$$\frac{D\Gamma}{Dt} = 0 \quad (4.11)$$

which says that the time rate of change of circulation around a closed curve consisting of the same fluid elements is zero. Equation (4.11) along with its supporting discussion is called *Kelvin's circulation theorem*.⁴ Its derivation from

⁴ Kelvin's theorem also holds for an inviscid compressible flow in the special case where $\rho = \rho(p)$; that is, the density is some single-valued function of pressure. Such is the case for isentropic flow, to be treated in later chapters.



(a) Fluid at rest relative to the airfoil



(b) Picture some moments after the start of the flow

Figure 4.21 The creation of the starting vortex and the resulting generation of circulation around the airfoil.

first principles is left as Problem 4.3. Also, recall our definition and discussion of a vortex sheet in Section 4.4. An interesting consequence of Kelvin's circulation theorem is proof that a stream surface which is a vortex sheet at some instant in time remains a vortex sheet for all times.

Kelvin's theorem helps to explain the generation of circulation around an airfoil, as follows. Consider an airfoil in a fluid at rest, as shown in Figure 4.21a. Because $V = 0$ everywhere, the circulation around curve C_1 is zero. Now start the flow in motion over the airfoil. Initially, the flow will tend to curl around the trailing edge, as explained in Section 4.5 and illustrated at the left of Figure 4.17. In so doing, the velocity at the trailing edge theoretically becomes infinite. In real life, the velocity tends toward a very large finite number. Consequently, during the very first moments after the flow is started, a thin region of very large velocity gradients (and therefore high vorticity) is formed at the trailing edge. This high-vorticity region is fixed to the same fluid elements, and consequently it is flushed downstream as the fluid elements begin to move downstream from the trailing edge. As it moves downstream, this thin sheet of intense vorticity is unstable, and it tends to roll up and form a picture similar to a point vortex. This vortex is called the *starting vortex* and is sketched in Figure 4.21b. After the flow around the airfoil has come to a steady state where the flow leaves the trailing edge smoothly (the Kutta condition), the high velocity gradients at the trailing edge disappear and vorticity is no longer produced at that point. However, the starting vortex has already been formed during the starting process, and it moves steadily downstream with the flow forever after. Figure 4.21b shows the flow field sometime after steady flow has

been achieved over the airfoil, with the starting vortex somewhere downstream. The fluid elements that initially made up curve C_1 in Figure 4.21a have moved downstream and now make up curve C_2 , which is the complete circuit $abcta$ shown in Figure 4.21b. Thus, from Kelvin's theorem, the circulation Γ_2 around curve C_2 (which encloses both the airfoil and the starting vortex) is the same as that around curve C_1 , namely, zero. $\Gamma_2 = \Gamma_1 = 0$. Now let us subdivide C_2 into two loops by making the cut bd , thus forming curves C_3 (circuit bcd) and C_4 (circuit $abda$). Curve C_3 encloses the starting vortex, and curve C_4 encloses the airfoil. The circulation Γ_3 around curve C_3 is due to the starting vortex; by inspecting Figure 4.21b, we see that Γ_3 is in the counterclockwise direction (i.e., a negative value). The circulation around curve C_4 enclosing the airfoil is Γ_4 . Since the cut bd is common to both C_3 and C_4 , the sum of the circulations around C_3 and C_4 is simply equal to the circulation around C_2 :

$$\Gamma_3 + \Gamma_4 = \Gamma_2$$

However, we have already established that $\Gamma_2 = 0$. Hence,

$$\Gamma_4 = -\Gamma_3$$

that is, the circulation around the airfoil is equal and opposite to the circulation around the starting vortex.

This brings us to the summary as well as the crux of this section. As the flow over an airfoil is started, the large velocity gradients at the sharp trailing edge result in the formation of a region of intense vorticity which rolls up downstream of the trailing edge, forming the starting vortex. This starting vortex has associated with it a counterclockwise circulation. Therefore, as an equal-and-opposite reaction, a clockwise circulation around the airfoil is generated. As the starting process continues, vorticity from the trailing edge is constantly fed into the starting vortex, making it stronger with a consequent larger counterclockwise circulation. In turn, the clockwise circulation around the airfoil becomes stronger, making the flow at the trailing edge more closely approach the Kutta condition, thus weakening the vorticity shed from the trailing edge. Finally, the starting vortex builds up to just the right strength such that the equal-and-opposite clockwise circulation around the airfoil leads to smooth flow from the trailing edge (the Kutta condition is exactly satisfied). When this happens, the vorticity shed from the trailing edge becomes zero, the starting vortex no longer grows in strength, and a steady circulation exists around the airfoil.

4.7 CLASSICAL THIN AIRFOIL THEORY: THE SYMMETRIC AIRFOIL

Some experimentally observed characteristics of airfoils and a philosophy for the theoretical prediction of these characteristics have been discussed in the preceding sections. Referring to our chapter road map in Figure 4.7, we have now completed the central branch. In this section, we move to the right-hand branch